Progress In Electromagnetics Research, PIER 23, 79–105, 1999

SCATTERING OF PLANE WAVES ON FINITE CYLINDERS WITH NON-CIRCULAR CROSS-SECTIONS

T. Rother, S. Havemann, and K. Schmidt

Remote Sensing Ground Station Neustrelitz
German Aerospace Research Establishment
Kalkhorstweg 53, D-17235 Neustrelitz, Germany

1. INTRODUCTION

Since some years, a growing interest in scattering of electromagnetic waves on more realistic geometries than represented by spheres and infinitely extended circular cylinders can be stated. In remote sensing, for instance, there is an urgent need to learn more about the scattering characteristics of hexagonal ice crystals which form basic constituents of cirrus clouds [1–9]. So far, ice crystals with moderate size-parameters, where ray-tracing techniques [10–12] can not be applied, have been modeled mainly by finitely extended circular cylinders or prolate/oblate spheroids [13–15]. Especially the exact T-matrix method was used in these calculations. In recent years, Finite-Difference methods have been applied to infinite and finite hexagonal

cylinders, like the Finite-Difference Time-Domain (FDTD) technique, for instance [17–19]. These methods have the conceptual disadvantage that a finite discretization volume is required. Therefore, absorbing boundary conditions must be introduced which allow only an approximate fulfillment of the non-local radiation condition. Moreover, orientation averaging becomes more complicated than in the T-matrix approach, and, it is known that spurious solutions can occur which have to be rejected in an additional process. These difficulties are overcome by the Discretized Mie Formalism (DMF) [20]. It was developed to deal with scatterers having non-separable boundary surfaces. In using the Method of Lines [21] to solve the Helmholtz equation belonging to the scattering problem, this method can be thought of as a synthesis of the well-known Mie theory and Finite-Difference methods. Like the Mie theory it analytically incorporates the regularity inside the scatterer and the radiation condition at infinity. As a result, the final calculation can be restricted to the surface of the scatterer only. Recently it could be shown that the limiting behaviour of the Method of Lines results in a generalization of the SVM applicable to scatterers having a boundary surface which does not coincide with a constant coordinate line in the coordinate system under consideration [22, 23].

Infinitely extended cylinders are simpler in concept because they reduce the scattering problem to a two-dimensional one. However, they do not occur in nature. Therefore, deriving approximate solutions for finite cylindrical structures on the basis of the results for infinitely extended ones is a first step towards more realistic structures. A first application of this idea to circular cylinders was given in [24, 25] and is based on Huygens' principle. For that it is assumed that the surface fields on the mantle of a sufficiently long finite cylinder are approximately those of the infinite one, and that any contribution from the top and bottom faces can be neglected. However, only perpendicularly incident fields with respect to the cylinder axis have been considered. An extension to oblique incidence can be found in [26, 27]. In this paper, we will discuss the extension to non-circular cross-sections.

First, the scattered field of infinite cylinders with non-circular cross sections is calculated by use of the generalization of the SVM. This allows us to determine the surface fields exactly. Next, the vectorial formulation of Huygens' principle is used to derive an approximation of the scattered far field, and any related quantities of interest of the corresponding finite cylinder. In applying Huygens' principle, the surface

integration over the actual mantle surface is replaced by an integration over the mantle of the smallest circular cylinder circumscribing the non-circular one. This allows an analytical calculation of the total surface integration and results in analytical expressions for the scattering amplitudes that can be readily implemented in computer programs. In a third part we will discuss the range of applicability of the approximation. This is achieved by a comparison with exact results for finite circular cylinders. Finally, results for finite hexagonal columns in different size parameter regions are presented.

2. SCATTERING ON INFINITE CYLINDERS WITH NON-CIRCULAR CROSS-SECTIONS

2.1 Formulation of the Problem in Cylindrical Coordinates

Throughout this paper we assume homogeneous, isotropic, and in general absorbing dielectric cylinders. Moreover, we will only consider monochromatic electromagnetic fields with a time-dependence $e^{-j\omega t}$. The internal and scattered electromagnetic fields are decomposed into transverse electric (TE) and transverse magnetic (TM) parts with respect to the z'-direction. $\{x',\ y',\ z'\}$ represent the coordinates of the body frame with z' being the cylindrical axis. Each part can be derived from a scalar potential, Π_e and Π_m, so that the following relations hold in cylindrical coordinates:

$$E_{z'} = \frac{j}{\omega\epsilon}\left[\frac{\partial^2\Pi_e}{\partial z'^2} + k^2\Pi_e\right] \tag{1}$$

$$E_{\rho'} = \frac{j}{\omega\epsilon}\frac{\partial^2\Pi_e}{\partial z'\partial\rho'} + \frac{1}{\rho'}\frac{\partial\Pi_m}{\partial\phi'} \tag{2}$$

$$E_{\phi'} = \frac{j}{\omega\epsilon}\frac{1}{\rho'}\frac{\partial^2\Pi_e}{\partial z'\partial\phi'} - \frac{\partial\Pi_m}{\partial\rho'} \tag{3}$$

$$H_{z'} = -\frac{j}{\omega\mu_0}\left[\frac{\partial^2\Pi_m}{\partial z'^2} + k^2\Pi_m\right] \tag{4}$$

$$H_{\rho'} = -\frac{j}{\omega\mu_0}\frac{\partial^2\Pi_m}{\partial z'\partial\rho'} + \frac{1}{\rho'}\frac{\partial\Pi_e}{\partial\phi'} \tag{5}$$

$$H_{\phi'} = -\frac{j}{\omega\mu_0}\frac{1}{\rho'}\frac{\partial^2\Pi_m}{\partial z'\partial\phi'} - \frac{\partial\Pi_e}{\partial\rho'} \tag{6}$$

Please note that in the outer region $\epsilon = \epsilon_0$ is assumed whereas $\epsilon = \epsilon_s' + j\epsilon_s''$ is used for the inner region. The potentials have to fulfill the scalar Helmholtz equation:

$$\nabla^2 \Pi_{e/m} + k^2 \rho'^2 \Pi_{e/m} = 0 \tag{7}$$

$$\nabla^2 = \rho' \frac{\partial}{\partial \rho'} \rho' \frac{\partial}{\partial \rho'} + \rho'^2 \frac{\partial^2}{\partial z'^2} + \frac{\partial^2}{\partial \phi'^2}. \tag{8}$$

The incident field is given in the laboratory frame denoted by $\{x, y, z\}$. It propagates along the positive z-axis, i.e., we have

$$\vec{E}_v^{inc} = \vec{e}_y E_0 e^{jk_0 z} \qquad \vec{H}_v^{inc} = -\vec{e}_x \frac{k_0}{\omega \mu_0} E_0 e^{jk_0 z} \tag{9}$$

$$\vec{E}_h^{inc} = -\frac{\omega \mu_0}{k_0} \vec{H}_v^{inc} \qquad \vec{H}_h^{inc} = \frac{k_0}{\omega \mu_0} \vec{E}_v^{inc} \tag{10}$$

for the horizontal (h) and vertical (v) polarization if the xz-plane is taken as the reference plane. In analogy to three-dimensional scatterers, the orientation of the cylinder is described by the Eulerian angles of rotation $\{\phi_p,\ \theta_p,\ \psi_p\}$ which transform the laboratory frame into the body frame (see Figure 1). This transformation is expressed by

$$\begin{pmatrix} x' \\ y' \\ z' \end{pmatrix} = \overline{\overline{A}} \cdot \begin{pmatrix} x \\ y \\ z \end{pmatrix} \tag{11}$$

with

$$\overline{\overline{A}} = \begin{pmatrix} \cos\phi_p \cos\theta_p \cos\psi_p - \sin\phi_p \sin\psi_p & \sin\phi_p \cos\theta_p \cos\psi_p + \cos\phi_p \sin\psi_p & -\sin\theta_p \cos\psi_p \\ -\cos\phi_p \cos\theta_p \sin\psi_p - \sin\phi_p \cos\psi_p & -\sin\phi_p \cos\theta_p \sin\psi_p + \cos\phi_p \cos\psi_p & \sin\theta_p \sin\psi_p \\ \cos\phi_p \sin\theta_p & \sin\phi_p \sin\theta_p & \cos\theta_p \end{pmatrix}. \tag{12}$$

After transition to cylindrical coordinates in the body frame we finally obtain for the components of the incident field:

$$E_{z',v}^{inc} = A_{32} E_0 e^{jk_0[\rho'(\cos\phi' A_{13} + \sin\phi' A_{23}) + z' \cos\theta_p]} \tag{13}$$

$$E_{\rho',v}^{inc} = \left[\cos\phi' A_{12} + \sin\phi' A_{22}\right]$$

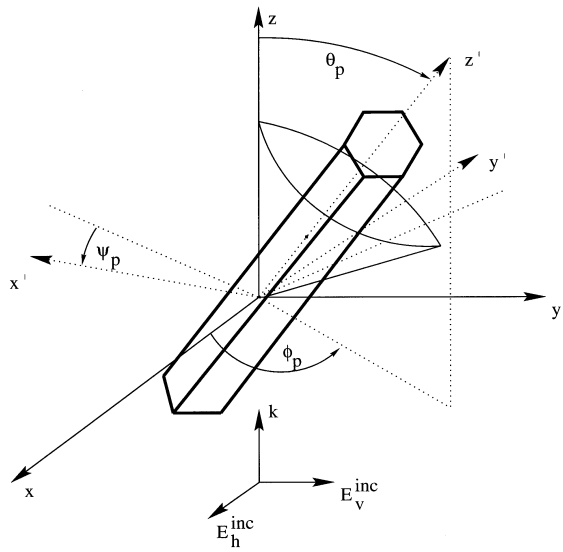

Figure 1. Scattering geometry: Laboratory frame $(x,\ y,\ z)$ and body frame $(x',\ y',\ z')$, related by an Eulerian transformation with the Eulerian angles $(\phi_p,\ \theta_p,\ \psi_p)$; Scattering cone at $\theta' = \theta_p$ in the body frame.

$$\cdot E_0 e^{jk_0[\rho'(\cos\phi' A_{13} + \sin\phi' A_{23}) + z'\cos\theta_p]} \tag{14}$$

$$E^{inc}_{\phi',v} = \left[(-\sin\phi')A_{12} + \cos\phi' A_{22}\right] \cdot E_0 e^{jk_0[\rho'(\cos\phi' A_{13} + \sin\phi' A_{23}) + z'\cos\theta_p]} \tag{15}$$

$$H^{inc}_{z',v} = -A_{31}\frac{k_0}{\omega\mu_0} E_0 e^{jk_0[\rho'(\cos\phi' A_{13} + \sin\phi' A_{23}) + z'\cos\theta_p]} \tag{16}$$

$$H^{inc}_{\rho',v} = -\left[\cos\phi' A_{11} + \sin\phi' A_{21}\right]\frac{k_0}{\omega\mu_0} \cdot E_0 e^{jk_0[\rho'(\cos\phi' A_{13} + \sin\phi' A_{23}) + z'\cos\theta_p]} \tag{17}$$

$$H^{inc}_{\phi',v} = \left[\sin\phi' A_{11} - \cos\phi' A_{21}\right]\frac{k_0}{\omega\mu_0} \cdot E_0 e^{jk_0[\rho'(\cos\phi' A_{13} + \sin\phi' A_{23}) + z'\cos\theta_p]}. \tag{18}$$

Now we can come to the crucial step of the analysis, the derivation of the characteristic equation system.

2.2 Application of the Separation of Variables Method to Non-Circular Cylinders

There exist different numerical approaches to analyze plane wave scattering on infinitely extended non-circular cylinders. Among them surface integral equation methods and the DMF are the most powerful ones, especially if orientation averaging becomes necessary [28–30]. That's what happens in remote sensing applications, for instance. Recently it could be shown that the discretization procedure of the DMF can be avoided, and that the SVM can be used directly [22, 23]. The following treatment of the infinitely extended non-circular cylinder is based on this formulation. Applying the well-known separation *ansatz* to the Helmholtz equation (7)/(8) provides the following series expansions for the scalar potentials belonging to the internal (index "int") and scattered (index "s") field:

$$\Pi_e^{int} = -\frac{j}{\omega\mu_0} E_0\, e^{jhz'} \sum_\alpha a_\alpha J_\alpha \left(\sqrt{k_s^2 - h^2}\rho'\right) e^{j\alpha\phi'} \tag{19}$$

$$\Pi_m^{int} = -\frac{j}{k_s} E_0\, e^{jhz'} \sum_\alpha b_\alpha J_\alpha \left(\sqrt{k_s^2 - h^2}\rho'\right) e^{j\alpha\phi'} \tag{20}$$

$$\Pi_e^{s} = -\frac{j}{\omega\mu_0} E_0\, e^{jhz'} \sum_\alpha c_\alpha H_\alpha^{(1)} \left(\sqrt{k_0^2 - h^2}\rho'\right) e^{j\alpha\phi'} \tag{21}$$

$$\Pi_m^{s} = -\frac{j}{k_0} E_0\, e^{jhz'} \sum_\alpha d_\alpha H_\alpha^{(1)} \left(\sqrt{k_0^2 - h^2}\rho'\right) e^{j\alpha\phi'}. \tag{22}$$

h is the separation constant for z'-separation, and it is related to the incident field as will be shown later. The Hankel functions of first kind fulfill the radiation condition in the outer region, and the Bessel functions ensure the regularity inside the scatterer. (19)–(22) together with (1)–(6) result in the corresponding expansions for the electromagnetic field components. To determine the unknown expansion coefficients $a_\alpha, b_\alpha, c_\alpha$, and d_α the continuity conditions

$$\vec{n} \times [\vec{E}^{int} - \vec{E}^{inc} - \vec{E}^{s}] = 0 \tag{23}$$

$$\vec{n} \times [\vec{H}^{int} - \vec{H}^{inc} - \vec{H}^{s}] = 0 \tag{24}$$

of the tangential field components at the scatterer surface are of special importance. $\vec{n}$ denotes the outward directed unit normal vector, and

is given by

$$\vec{n} = n_c \left(\vec{e}_{\rho'} - \frac{R'(\phi')}{R(\phi')} \vec{e}_{\phi'} \right) \tag{25}$$

$$n_c = \left\{ 1 + \left(\frac{R'(\phi')}{R(\phi')} \right)^2 \right\}^{-\frac{1}{2}} \tag{26}$$

for the non-circular and single-valued boundary surface $R(\phi')$. (23) and (24) can be rewritten into the four equations:

$$-E^{int}_{z'} + E^{s}_{z'} = -E^{inc}_{z'} \tag{27}$$

$$-\left[E^{int}_{\phi'} + \frac{R'(\phi')}{R(\phi')} E^{int}_{\rho'} \right] + \left[E^{s}_{\phi'} + \frac{R'(\phi')}{R(\phi')} E^{s}_{\rho'} \right] = -\left[E^{inc}_{\phi'} + \frac{R'(\phi')}{R(\phi')} E^{inc}_{\rho'} \right] \tag{28}$$

$$-H^{int}_{z'} + H^{s}_{z'} = -H^{inc}_{z'} \tag{29}$$

$$-\left[H^{int}_{\phi'} + \frac{R'(\phi')}{R(\phi')} H^{int}_{\rho'} \right] + \left[H^{s}_{\phi'} + \frac{R'(\phi')}{R(\phi')} H^{s}_{\rho'} \right] = -\left[H^{inc}_{\phi'} + \frac{R'(\phi')}{R(\phi')} H^{inc}_{\rho'} \right]. \tag{30}$$

Next we insert all the field components derived above into equations (27)–(30). In any practical calculation the expansion terms in (19)–(22) must be restricted to a finite number. Therefore, α runs from $-ncut, \ldots, ncut$, where $ncut$ has to be determined by appropriate convergence considerations. If we integrate each of the equations (27)–(30) with

$$\int_0^{2\pi} d\phi' e^{-j\beta\phi'}, \tag{31}$$

with β also running from $-ncut, \ldots, ncut$, we finally obtain the characteristic equation system

$$\begin{pmatrix} \overline{\overline{M}} & \overline{\overline{\emptyset}} & \overline{\overline{O}} & \overline{\overline{\emptyset}} \\ \overline{\overline{Q}} & \overline{\overline{R}} & \overline{\overline{S}} & \overline{\overline{T}} \\ \overline{\overline{\emptyset}} & -\frac{k_s}{k_0}\overline{\overline{M}} & \overline{\overline{\emptyset}} & -\overline{\overline{O}} \\ \frac{k_s}{k_0}\overline{\overline{R}} & -\frac{k_s}{k_0}\overline{\overline{Q}} & \overline{\overline{T}} & -\overline{\overline{S}} \end{pmatrix} \begin{pmatrix} \vec{a} \\ \vec{b} \\ \vec{c} \\ \vec{d} \end{pmatrix} = \begin{pmatrix} -\vec{e}^{(h/v)}_{z'} \\ -\vec{e}^{(h/v)}_{\phi',\rho'} \\ -\vec{h}^{(h/v)}_{z'} \\ -\vec{h}^{(h/v)}_{\phi',\rho'} \end{pmatrix} \tag{32}$$

to determine the unknown expansion coefficients. The elements of the block matrices in (32) are of the general form

$$Z_{\alpha\beta} = \int_0^{2\pi} Z_\alpha e^{j(\alpha-\beta)\phi'} d\phi', \tag{33}$$

with Z_α being one of the functions $M_\alpha,\ O_\alpha,\ Q_\alpha,\ R_\alpha,\ S_\alpha,\ T_\alpha$, which are given by:

$$M_\alpha = -\kappa_s^2 J_\alpha\left(\xi_s'\right) \tag{34}$$

$$O_\alpha = \kappa_0^2 H_\alpha^{(1)}\left(\xi_0'\right) \tag{35}$$

$$Q_\alpha = -j\kappa_s \frac{h}{k_s}\left(\frac{J_\alpha\left(\xi_s'\right)}{\xi_s'} j\alpha + \frac{R'(\phi')}{R(\phi')} J_\alpha'\left(\xi_s'\right)\right) \tag{36}$$

$$R_\alpha = -j\kappa_s\left(J_\alpha'\left(\xi_s'\right) - \frac{R'(\phi')}{R(\phi')}\frac{J_\alpha\left(\xi_s'\right)}{\xi_s'} j\alpha\right) \tag{37}$$

$$S_\alpha = j\kappa_0 \frac{h}{k_0}\left(\frac{H_\alpha^{(1)}\left(\xi_0'\right)}{\xi_0'} j\alpha + \frac{R'(\phi')}{R(\phi')} H_\alpha^{(1)'}\left(\xi_0'\right)\right) \tag{38}$$

$$T_\alpha = j\kappa_0\left(H_\alpha^{(1)'}\left(\xi_0'\right) - \frac{R'(\phi')}{R(\phi')}\frac{H_\alpha^{(1)}\left(\xi_0'\right)}{\xi_0'} j\alpha\right) \tag{39}$$

$$\kappa_{0/s} = \left(1 - \frac{h^2}{k_{0/s}^2}\right)^{\frac{1}{2}} \tag{40}$$

$$\xi_{0/s}' = \left(k_{0/s} - h^2\right)^{\frac{1}{2}} R(\phi'). \tag{41}$$

To fulfill the continuity conditions the z'-dependence of the internal, scattered and incident field must be identical. Therefore

$$h = k_0 \cos\theta_p \tag{42}$$

has to be used. The inhomogeneities on the right-hand side of (32) are nothing but the expansion coefficients of the tangential components of the incident field at the scatterer surface if expanded in terms of $e^{j\beta\phi'}$, i.e., we have:

$$e_{z_\beta'}^{(h/v)} = \int_0^{2\pi} e^{-j\beta\phi'} E_{z'}^{inc} d\phi' \tag{43}$$

$$e^{(h/v)}_{\phi',\rho'_\beta} = \int_0^{2\pi} e^{-j\beta\phi'} \left(E^{inc}_{\phi'} + \frac{R'(\phi')}{R(\phi')} E^{inc}_{\rho'} \right) d\phi' \tag{44}$$

$$h^{(h/v)}_{z'_\beta} = \int_0^{2\pi} e^{-j\beta\phi'} H^{inc}_{z'} d\phi' \tag{45}$$

$$h^{(h/v)}_{\phi',\rho'_\beta} = \int_0^{2\pi} e^{-j\beta\phi'} \left(H^{inc}_{\phi'} + \frac{R'(\phi')}{R(\phi')} H^{inc}_{\rho'} \right) d\phi'. \tag{46}$$

The only difference between the circular and non-circular cylinder is the fact that in the former case all block matrices of (32) become diagonal, due to the independence of Z_α of the ϕ'-coordinate. Then, the inversion of (32) can be performed analytically, and we obtain the well-known expansion coefficients of the circular cylinder. In the other case the block matrices become full matrices of the order $(2ncut + 1) \times (2ncut + 1)$, and the inversion must be performed numerically. But, there exists the possibility to reduce the numerical effort. It can be shown that in a fixed column "α" of each block matrix in (32) the elements decrease with increasing distance $|\alpha - \beta|$ from the main diagonal. This is seen from relation (33) which can be interpreted as an expansion of Z_α in terms of the functions $e^{jn\phi'}$, with $n = \alpha - \beta$. Therefore, each block matrix should be constructed in such a way that, starting with the main diagonal, the adjacent diagonals are added stepwise until convergence is achieved. Actual calculations have shown that only a few adjacent diagonals have to be taken into account if the boundary surface does not deviate too much from a circular one.

Once the coefficients have been determined the electromagnetic field for the infinitely extended cylinder is given at any point in space. The components of the scattered field on the mantle of the smallest circular cylinder, circumscribing this non-circular one, read as follows:

$$E^{surf}_{z'} = E_0 e^{jk_0 z' \cos\theta_p} \left(\sin^2\theta_p \right) \sum_\alpha c_\alpha H^{(1)}_\alpha(\xi') e^{j\alpha\phi'} \tag{47}$$

$$E^{surf}_{\rho'} = E_0 e^{jk_0 z' \cos\theta_p} \left(j \sin\theta_p \right) \cdot \sum_\alpha \left\{ (\cos\theta_p)\, c_\alpha H^{(1)\,\prime}_\alpha(\xi') - d_\alpha \frac{H^{(1)}_\alpha(\xi')}{\xi'} j\alpha \right\} e^{j\alpha\phi'} \tag{48}$$

$$E^{surf}_{\phi'} = E_0 e^{jk_0 z' \cos\theta_p} \left(j \sin\theta_p \right) \cdot \sum_\alpha \left\{ (\cos\theta_p)\, c_\alpha \frac{H^{(1)}_\alpha(\xi')}{\xi'} j\alpha + d_\alpha H^{(1)\,\prime}_\alpha(\xi') \right\} e^{j\alpha\phi'} \tag{49}$$

$$H_{z'}^{surf} = -\frac{k_0}{\omega\mu_0} E_0 e^{jk_0 z' \cos\theta_p} \left(\sin^2\theta_p\right) \sum_\alpha d_\alpha H_\alpha^{(1)}(\xi') e^{j\alpha\phi'} \tag{50}$$

$$H_{\rho'}^{surf} = -\frac{k_0}{\omega\mu_0} E_0 e^{jk_0 z' \cos\theta_p} \left(j\sin\theta_p\right) \cdot \sum_\alpha \left\{ \left(\cos\theta_p\right) d_\alpha H_\alpha^{(1)\,\prime}(\xi') + c_\alpha \frac{H_\alpha^{(1)}(\xi')}{\xi'} j\alpha \right\} e^{j\alpha\phi'} \tag{51}$$

$$H_{\phi'}^{surf} = -\frac{k_0}{\omega\mu_0} E_0 e^{jk_0 z' \cos\theta_p} \left(j\sin\theta_p\right) \cdot \sum_\alpha \left\{ \left(\cos\theta_p\right) d_\alpha \frac{H_\alpha^{(1)}(\xi')}{\xi'} j\alpha - c_\alpha H_\alpha^{(1)\,\prime}(\xi') \right\} e^{j\alpha\phi'}, \tag{52}$$

with $\xi' = k_0 R_{min} \sin\theta_p$. R_{min} is the radius of the smallest circumscribing cylinder.

These are the input quantities for our approximation we want to derive in the next chapter.

3. AN APPROXIMATE SOLUTION FOR SCATTERING ON FINITE NON-CIRCULAR CYLINDERS

For the following considerations, Huygens' principle serves as a starting point. It states that the electromagnetic fields are uniquely determined at any point in space if the tangential electric and magnetic field components on an arbitrary closed surface are given. In vector form it reads as follows (e.g., [31])

$$\vec{E}^s\left(\vec{r'}\right) = \oint_{\underline{S}} \underline{dS} \left\{ j\omega\mu_0 \overline{\overline{G}}\left(\vec{r'}, \vec{\underline{r}'}\right) \left[\vec{n} \times \vec{H}^{surf}\left(\vec{\underline{r}'}\right)\right] + \left[\nabla \times \overline{\overline{G}}\left(\vec{r'}, \vec{\underline{r}'}\right)\right] \left[\vec{n} \times \vec{E}^{surf}\left(\vec{\underline{r}'}\right)\right] \right\} \tag{53}$$

In our specific problem $\vec{E}^s(\vec{r'})$ represents the scattered field of the finite cylinder we are looking for. Consequently, the tangential surface fields $[\vec{n} \times \vec{E}^{surf}(\vec{\underline{r}'})]$ and $[\vec{n} \times \vec{H}^{surf}(\vec{\underline{r}'})]$, occurring on the right hand side of (53), are those of the finite structure. According to [24–27], these surface fields are approximated by those of the corresponding infinite cylinder given in (47)–(52), thus neglecting the contributions from the top and bottom faces. Cylindrical coordinates $\{\underline{\rho}', \underline{\phi}', \underline{z}'\}$ are chosen for performing the surface integration since they are matched

best to the geometry under consideration. Due to the usage of the circumscribing circular cylinder $\vec{n}$ reduces to $\vec{n} = \vec{e}_{\rho'}$ in (53).

The Green's dyad $\overline{\overline{G}}(\vec{r'}, \underline{\vec{r}'})$, occurring in Huygens' principle (53), is given by [31]

$$\overline{\overline{G}}\left(\vec{r'}, \underline{\vec{r}'}\right) = \left\{\overline{\overline{I}} + \frac{1}{k_0^2}\nabla\nabla\right\} g_0\left(\vec{r'}, \underline{\vec{r}'}\right) \tag{54}$$

with the scalar Green's function

$$g_0\left(\vec{r'}, \underline{\vec{r}'}\right) = \frac{e^{jk_0\left(\vec{r'} - \underline{\vec{r}'}\right)}}{4\pi\left|\vec{r'} - \underline{\vec{r}'}\right|}. \tag{55}$$

Since we are only interested in scattering quantities that are defined in the far field of the particle, the far field approximation of $\vec{E}^s(\vec{r'})$ is considered. In this approximation, the scattered field of any finite obstacle represents outgoing spherical waves which are best described in spherical coordinates $\{r', \theta', \phi'\}$. Thus, we obtain the following far field expression for the dyadic Green's function which is the only quantity on the right hand side of (53) that depends on the observation point $\vec{r'}$:

$$\overline{\overline{G}}\left(\vec{r'}, \underline{\vec{r}'}\right) = \left\{\vec{e_{\theta'}}\vec{e_{\theta'}} + \vec{e_{\phi'}}\vec{e_{\phi'}}\right\} \frac{e^{jk_0 r'}}{4\pi r'} e^{-jk_0 \vec{e_{r'}} \cdot \underline{\vec{r}'}}. \tag{56}$$

It's straightforward to show from (56) that

$$\left[\nabla \times \overline{\overline{G}}\left(\vec{r'}, \underline{\vec{r}'}\right)\right] = \left\{\vec{e_{\phi'}}\vec{e_{\theta'}} - \vec{e_{\theta'}}\vec{e_{\phi'}}\right\} (jk_0) \frac{e^{jk_0 r'}}{4\pi r'} e^{-jk_0 \vec{e_{r'}} \cdot \underline{\vec{r}'}}. \tag{57}$$

The scalar product $\vec{e_{r'}} \cdot \underline{\vec{r}'}$ in equations (56) and (57) between vectors given in spherical and cylindrical coordinates provides

$$\vec{e_{r'}} \cdot \underline{\vec{r}'} = R_{min} \sin\theta' \cos\left(\underline{\phi'} - \phi'\right) + \underline{z'} \cos\theta'. \tag{58}$$

Similar scalar products are obtained when inserting equations (47)–(52) and (56)–(57) into (53):

$$\vec{e}_{\theta'} \cdot \vec{e}_{\underline{\phi'}} = \cos\theta' \sin\left(\underline{\phi'} - \phi'\right) \tag{59}$$

$$\vec{e}_{\theta'} \cdot \vec{e}_{\underline{z'}} = -\sin\theta' \tag{60}$$

$$\vec{e}_{\phi'} \cdot \vec{e}_{\underline{\phi'}} = \cos\left(\underline{\phi'} - \phi'\right) \tag{61}$$

$$\vec{e}_{\phi'} \cdot \vec{e}_{\underline{z'}} = 0\,. \tag{62}$$

Now we are able to calculate the surface integral of Huygens' principle. After performing the $\underline{z}'$-integration over the finite cylinder length l the following $\underline{\phi}'$-integrals remain:

$$I_\alpha^s = \int_{\underline{\phi}'=0}^{\underline{\phi}'=2\pi} d\underline{\phi}' e^{-jk_0 R_{min}\sin\theta'\cos\left(\underline{\phi}'-\phi'\right)} \sin\left(\underline{\phi}'-\phi'\right) e^{j\alpha\phi'} \tag{63}$$

$$I_\alpha^c = \int_{\underline{\phi}'=0}^{\underline{\phi}'=2\pi} d\underline{\phi}' e^{-jk_0 R_{min}\sin\theta'\cos\left(\underline{\phi}'-\phi'\right)} \cos\left(\underline{\phi}'-\phi'\right) e^{j\alpha\phi'} \tag{64}$$

$$I_\alpha = \int_{\underline{\phi}'=0}^{\underline{\phi}'=2\pi} d\underline{\phi}' e^{-jk_0 R_{min}\sin\theta'\cos\left(\underline{\phi}'-\phi'\right)} e^{j\alpha\phi'}. \tag{65}$$

They can be analytically calculated resulting in

$$I_\alpha^s = -2\pi(-j)^\alpha \alpha \frac{J_\alpha(\xi_I')}{\xi_I'} e^{j\alpha\phi'} \tag{66}$$

$$I_\alpha^c = -2\pi(-j)^{\alpha+1} J_\alpha'(\xi_I') e^{j\alpha\phi'} \tag{67}$$

$$I_\alpha = 2\pi(-j)^\alpha J_\alpha(\xi_I') e^{j\alpha\phi'} \tag{68}$$

$$\xi_I' = k_0 R_{min}\sin\theta'. \tag{69}$$

Finally, the following approximation for the scattered far field of a finite cylinder with an arbitrary cross-section in the body frame is obtained:

$$\begin{aligned}
\vec{E}^s(\vec{r'}) = E_0 \frac{e^{jk_0 r'}}{r'} \frac{j}{4\pi} \xi' \left[l \frac{\sin\left(\frac{k_0 l}{2}\left(\cos\theta_p - \cos\theta'\right)\right)}{\frac{k_0 l}{2}\left(\cos\theta_p - \cos\theta'\right)} \right] \\
\times \left(\vec{e}_{\theta'} \left\{ \sum_\alpha \sin\theta_p H_\alpha^{(1)}(\xi') \left(\cos\theta' d_\alpha I_\alpha^s - c_\alpha I_\alpha^c\right) \right.\right. \\
\left. + j\sin\theta' \left(-j\alpha\cos\theta_p d_\alpha \frac{H_\alpha^{(1)}(\xi')}{\xi'} + c_\alpha H_\alpha^{(1)'}(\xi') \right) I_\alpha \right\} \\
+ \vec{e}_{\phi'} \left\{ \sum_\alpha \sin\theta_p H_\alpha^{(1)}(\xi') \left(-\cos\theta' c_\alpha I_\alpha^s + d_\alpha I_\alpha^c\right) \right. \\
\left.\left. + j\sin\theta' \left(j\alpha\cos\theta_p c_\alpha \frac{H_\alpha^{(1)}(\xi')}{\xi'} + d_\alpha H_\alpha^{(1)'}(\xi') \right) I_\alpha \right\} \right).
\end{aligned} \tag{70}$$

This is in correspondence with the result published in [26] but with coefficients c_α and d_α obtained from the non-circular cylinder.

From infinitely extended cylinders it is known that the scattered field concentrates on a cone defined by θ_p (see Figure 1). Our approximation reveals a similar behaviour if increasing the cylinder length l up to infinity. In this case the l-dependent factor in (70) becomes

$$\lim_{l\to\infty}\left[l\frac{\sin\left(\frac{k_0 l}{2}\left(\cos\theta_p-\cos\theta'\right)\right)}{\frac{k_0 l}{2}\left(\cos\theta_p-\cos\theta'\right)}\right]=\frac{2\pi}{k_0\sin\theta'}\,\delta(\theta'-\theta_p)\,. \tag{71}$$

Of course, the calculation of differential scattering cross-sections makes no sense due to the δ-dependence of the field components. However, reasonable total cross-sections are obtained by integration over θ'. Now, let's see what happens with (70) if $\theta'=\theta_p$ is chosen for a finite length. By use of the relation

$$J_\alpha(\chi)\,H_\alpha^{(1)'}(\chi)-J'_\alpha(\chi)\,H_\alpha^{(1)}(\chi)=\frac{2j}{\pi\chi}\,, \tag{72}$$

we end up with

$$\vec{E}^s(\vec{r'})=E_0\frac{e^{jk_0r'}}{r'}\frac{\sin\theta_p}{\pi}l\sum_\alpha(-j)^{\alpha+1}\left(\vec{e}_{\theta'}c_\alpha+\vec{e}_{\phi'}d_\alpha\right)e^{j\alpha\phi'}\,. \tag{73}$$

Apart from the radial dependence, the remaining expression is proportional to what is known from the infinitely extended cylinder (see [32] and [20]).

The expressions derived so far are valid within the body frame. Since all scattering quantities are considered within the laboratory frame, the field in equation (70) has to be transformed back into this system by

$$E_\theta^s=W_{11}E_{\theta'}^s+W_{12}E_{\phi'}^s \tag{74}$$

$$E_\phi=W_{21}E_{\theta'}^s+W_{22}E_{\phi'}^s\,. \tag{75}$$

Moreover, the scattering quantities will be defined in the reference plane (xz-plane with $\phi=0$ and π) so that the functions $W_{ij}(i,j=1,2)$ are given by

$$
\begin{aligned}
W_{11} &= \cos\theta\cos\phi A_{11}\cos\theta'\cos\phi' - \sin\theta A_{13}\cos\theta'\cos\phi' \\
&\quad + \cos\theta\cos\phi A_{21}\cos\theta'\sin\phi' - \sin\theta A_{23}\cos\theta'\sin\phi' \\
&\quad - \cos\theta\cos\phi A_{31}\sin\theta' + \sin\theta A_{33}\sin\theta' \qquad (76)\\
W_{12} &= -\cos\theta\cos\phi A_{11}\sin\phi' + \sin\theta A_{13}\sin\phi' \\
&\quad + \cos\theta\cos\phi A_{21}\cos\phi' - \sin\theta A_{23}\cos\phi' \qquad (77)\\
W_{21} &= \cos\phi A_{12}\cos\theta'\cos\phi' + \cos\phi A_{22}\cos\theta'\sin\phi' \\
&\quad - \cos\phi A_{32}\sin\theta' \qquad (78)\\
W_{22} &= -\cos\phi A_{12}\sin\phi' + \cos\phi A_{22}\cos\phi' \,. \qquad (79)
\end{aligned}
$$

Again, the $A_{ij}(i,j=1,2,3)$ are the elements of the Euler matrix (12). The corresponding variables transformation reads as follows:

$$
\theta'(\theta,\phi) = \arctan \left[\frac{((A_{11}\sin\theta\cos\phi + A_{13}\cos\theta)^2 + (A_{21}\sin\theta\cos\phi + A_{23}\cos\theta)^2)^{1/2}}{A_{31}\sin\theta\cos\phi + A_{33}\cos\theta} \right] \qquad (80)
$$

$$
\phi'(\theta,\phi) = \arctan\left[\frac{A_{21}\sin\theta\cos\phi + A_{23}\cos\theta}{A_{11}\sin\theta\cos\phi + A_{13}\cos\theta}\right] . \qquad (81)
$$

Now we define horizontally and vertically polarized components of the scattered far field with respect to the reference plane,

$$
\begin{aligned}
E_h^s &= E_\theta^s \qquad (82)\\
E_v^s &= E_\phi^s \,. \qquad (83)
\end{aligned}
$$

Then, the scattering amplitude matrix $\overline{\overline{f}}$ that relates these components to the polarized incident field (9) and (10) by the definition

$$
\begin{pmatrix} E_h^s \\ \\ E_v^s \end{pmatrix} = \frac{e^{jk_0 r}}{r} \cdot \overline{\overline{f}} \cdot \begin{pmatrix} E_h^{inc} \\ \\ E_v^{inc} \end{pmatrix} \quad \text{with} \quad \overline{\overline{f}} = \begin{pmatrix} f_{hh} & f_{hv} \\ \\ f_{vh} & f_{vv} \end{pmatrix} \qquad (84)
$$

has within our approximation the form:

$$f_{hh}(\theta) = \frac{j}{4\pi}\xi' \left[l \frac{\sin\left(\frac{k_0 l}{2}\left(\cos\theta_p - \cos\theta'\right)\right)}{\frac{k_0 l}{2}\left(\cos\theta_p - \cos\theta'\right)} \right] \sum_{\alpha} \left(W_{11} d_{\alpha}^{(h)} - W_{12} c_{\alpha}^{(h)} \right)$$
$$\cdot \left\{ \sin\theta_p H_{\alpha}^{(1)}(\xi') \cos\theta' I_{\alpha}^{s} + \alpha \sin\theta' \cos\theta_p \frac{H_{\alpha}^{(1)}(\xi')}{\xi'} I_{\alpha} \right\}$$
$$- \left(W_{11} c_{\alpha}^{(h)} + W_{12} d_{\alpha}^{(h)} \right) \left\{ \sin\theta_p H_{\alpha}^{(1)}(\xi') I_{\alpha}^{c} - j \sin\theta' H_{\alpha}^{(1)'}(\xi') I_{\alpha} \right\} \tag{85}$$

$$f_{hv}(\theta) = \frac{j}{4\pi}\xi' \left[l \frac{\sin\left(\frac{k_0 l}{2}\left(\cos\theta_p - \cos\theta'\right)\right)}{\frac{k_0 l}{2}\left(\cos\theta_p - \cos\theta'\right)} \right] \sum_{\alpha} \left(W_{11} d_{\alpha}^{(v)} - W_{12} c_{\alpha}^{(v)} \right)$$
$$\cdot \left\{ \sin\theta_p H_{\alpha}^{(1)}(\xi') \cos\theta' I_{\alpha}^{s} + \alpha \sin\theta' \cos\theta_p \frac{H_{\alpha}^{(1)}(\xi')}{\xi'} I_{\alpha} \right\}$$
$$- \left(W_{11} c_{\alpha}^{(v)} + W_{12} d_{\alpha}^{(v)} \right) \left\{ \sin\theta_p H_{\alpha}^{(1)}(\xi') I_{\alpha}^{c} - j \sin\theta' H_{\alpha}^{(1)'}(\xi') I_{\alpha} \right\} \tag{86}$$

$$f_{vh}(\theta) = \frac{j}{4\pi}\xi' \left[l \frac{\sin\left(\frac{k_0 l}{2}\left(\cos\theta_p - \cos\theta'\right)\right)}{\frac{k_0 l}{2}\left(\cos\theta_p - \cos\theta'\right)} \right] \sum_{\alpha} \left(W_{21} d_{\alpha}^{(h)} - W_{22} c_{\alpha}^{(h)} \right)$$
$$\cdot \left\{ \sin\theta_p H_{\alpha}^{(1)}(\xi') \cos\theta' I_{\alpha}^{s} + \alpha \sin\theta' \cos\theta_p \frac{H_{\alpha}^{(1)}(\xi')}{\xi'} I_{\alpha} \right\}$$
$$- \left(W_{21} c_{\alpha}^{(h)} + W_{22} d_{\alpha}^{(h)} \right) \left\{ \sin\theta_p H_{\alpha}^{(1)}(\xi') I_{\alpha}^{c} - j \sin\theta' H_{\alpha}^{(1)'}(\xi') I_{\alpha} \right\} \tag{87}$$

$$f_{vv}(\theta) = \frac{j}{4\pi}\xi' \left[l \frac{\sin\left(\frac{k_0 l}{2}\left(\cos\theta_p - \cos\theta'\right)\right)}{\frac{k_0 l}{2}\left(\cos\theta_p - \cos\theta'\right)} \right] \sum_{\alpha} \left(W_{21} d_{\alpha}^{(v)} - W_{22} c_{\alpha}^{(v)} \right)$$

$$\cdot \left\{ \sin\theta_p H_\alpha^{(1)}(\xi') \cos\theta' I_\alpha^s + \alpha \sin\theta' \cos\theta_p \frac{H_\alpha^{(1)}(\xi')}{\xi'} I_\alpha \right\}$$
$$- \left(W_{21} c_\alpha^{(v)} + W_{22} d_\alpha^{(v)} \right) \left\{ \sin\theta_p H_\alpha^{(1)}(\xi') I_\alpha^c - j \sin\theta' H_\alpha^{(1)'}(\xi') I_\alpha \right\} \tag{88}$$

Note that the amplitudes are functions of the scattering angle θ in the laboratory frame by the relations (76)–(81) for a fixed particle orientation. All other scattering quantities of interest can be calculated on the basis of the matrix $\overline{\overline{f}}$.

It is possible to compare f_{hh} and f_{vv} with the results derived by van de Hulst [24] for perpendicular incidence on finitely approximated circular cylinders. For this, we have to consider the special orientation ($\phi_p = \theta_p = \pi/2$). Together with the restriction to the scattering plane ($\phi = 0$ and π) it follows that $\theta' = \pi/2$. Taking this in (85) and (88) into account, and using (72) we get:

$$f_{hh}(\theta) = \mp \frac{l}{\pi} \sum_\alpha (-j)^{\alpha+1} d_\alpha^{(h)} e^{j\alpha(\pm\theta - \psi_p)} \tag{89}$$

$$f_{vv}(\theta) = \mp \frac{l}{\pi} \sum_\alpha (-j)^{\alpha+1} c_\alpha^{(v)} e^{j\alpha(\pm\theta - \psi_p)}. \tag{90}$$

The upper sign holds for $\phi = 0$, and the lower for $\phi = \pi$. These expressions are proportional to van de Hulst's amplitude function S.

4. VERIFICATION AND APPLICATION OF THE APPROXIMATION

To estimate the approximation derived in the previous chapter the finite circular cylinder can be used as a benchmark geometry. Due to its axisymmetric structure, a rigorous analysis is possible by application of the T-matrix approach in spherical coordinates, for instance. Exact results for circular cylinders with different length can be found in [13, 14, 33]. These are taken for a comparison of our approximation. The size parameter is $k_0 \cdot a = 2.75$, and for the refractive index we have $n = 1.31$. This refractive index is a representative value for light scattering on pure ice crystals in the visible. Both, fixed and random orientations were considered. In the first case, the cylinder

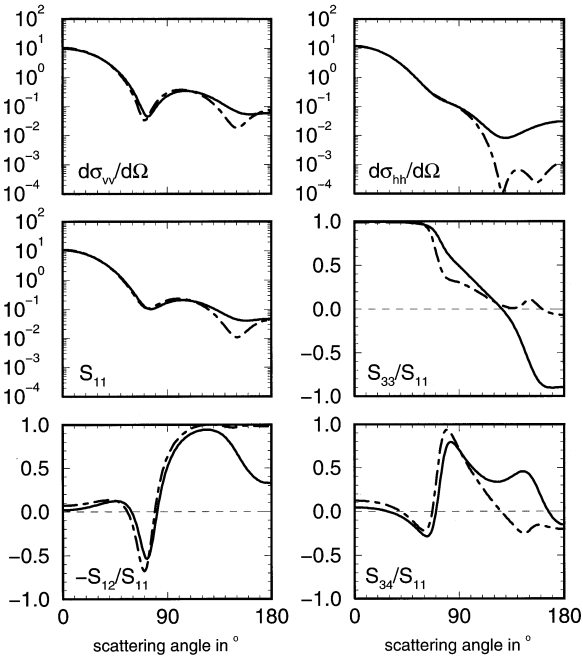

Figure 2. Differential scattering cross-sections $d\sigma_{vv}/d\Omega$ and $d\sigma_{hh}/d\Omega$ and the elements of the Stokes matrix S for a finite circular cylinder with its axis perpendicular to the direction of the scattering plane ($\phi_p = \pi/2,\ \theta_p = \pi/2$). Aspect ratio: 1.0, size parameter: 2.75, refractive index: 1.31 (–: exact, - · -: approximation).

axis is oriented perpendicularly to the reference plane, i.e. $\phi_p = \pi/2$ and $\theta_p = \pi/2$. Figures 2–4 show a comparison of results obtained by the exact method and the approximation for three different aspect ratios (1.0, 3.0, and 5.0). Please note that, in what follows, the aspect ratio is defined as the ratio of the cylindrical length to the largest diameter of the cross-section. The differential scattering cross-sections $d\sigma_{vv}/d\Omega$ and $d\sigma_{hh}/d\Omega$ as well as the elements of the Stokes matrix S are defined according to [14, 33]. For the special single scattering orientation in Figures 2–4 the cross polarized differential scattering cross-sections vanish so that the Stokes matrix element S_{11} reduces to $S_{11} = (d\sigma_{vv}/d\Omega + d\sigma_{hh}/d\Omega)/2$. Additionally, only four elements of the Stokes matrix are non-zero. Furthermore, the results obtained within the approximation for this orientation are independent of the

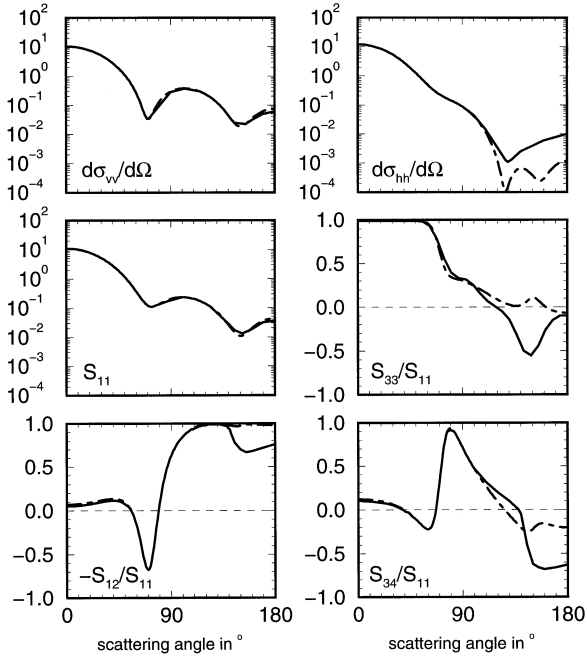

Figure 3. Same as Figure 2, but for an aspect ratio of 3.0.

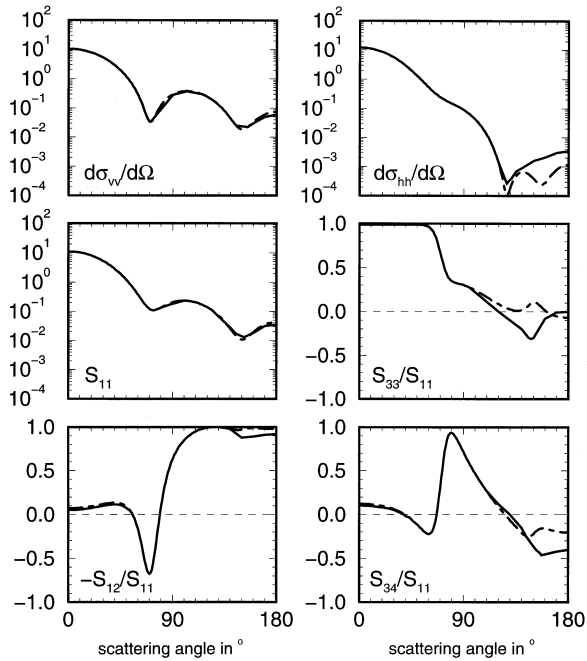

Figure 4. Same as Figure 2, but for an aspect ratio of 5.0.

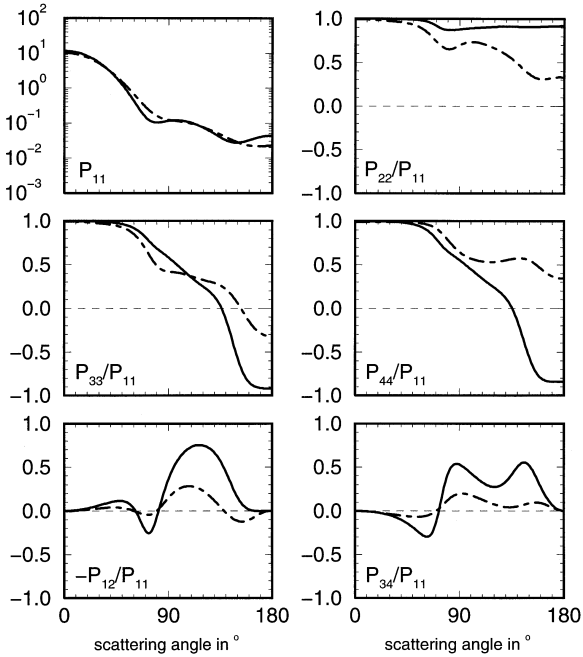

Figure 5. Elements of the phase matrix for randomly oriented finite circular cylinders with same parameters as used in Figure 2 (–: exact, - · -: approximation).

aspect ratio and equal to those of the corresponding infinite cylinder. For an aspect ratio of 1.0 (Figure 2), differences between the approximate results and those of the exact method can be especially observed in the back scattering region. These differences vanish to a great extent at the aspect ratio of 3.0 (Figure 3) and become even smaller if 5.0 is chosen (Figure 4). This indicates that the approximation becomes better with increasing aspect ratio at a given size parameter. The six non-zero phase matrix elements for random orientation, presented in the Figures 5-7, show a similar behaviour. We find again the tendency that, the greater the aspect ratio the better the approximation matches to the exact results. For an aspect ratio of 3.0, the differences between the exact phase function and our approximation may already be neglectable for many applications, as can be seen from Figure 6. In this figure there is also given the approximation used in [13]. It shows stronger deviations from the exact phase function than ours.

Now, lets turn to the hexagonal cylinder. A circular cylinder with an aspect ratio of 3.0, a size parameter of $k_0 \cdot a = 2.75$, and the

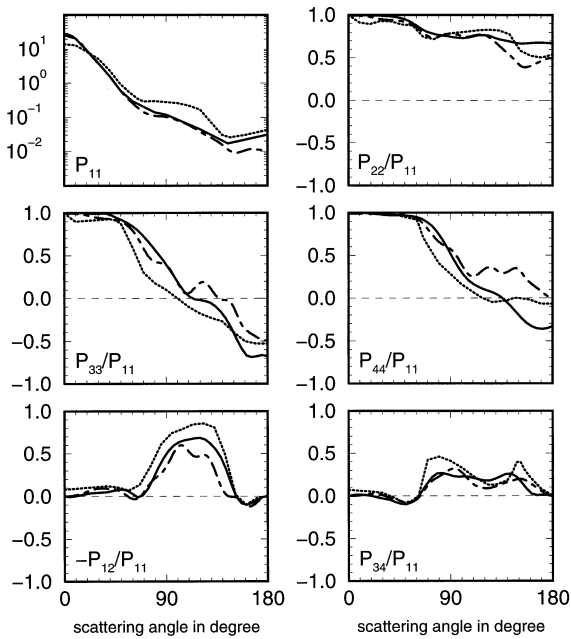

Figure 6. Same as Figure 5, but for an aspect ratio of 3.0. The approximation used in [13] is additionally shown (···).

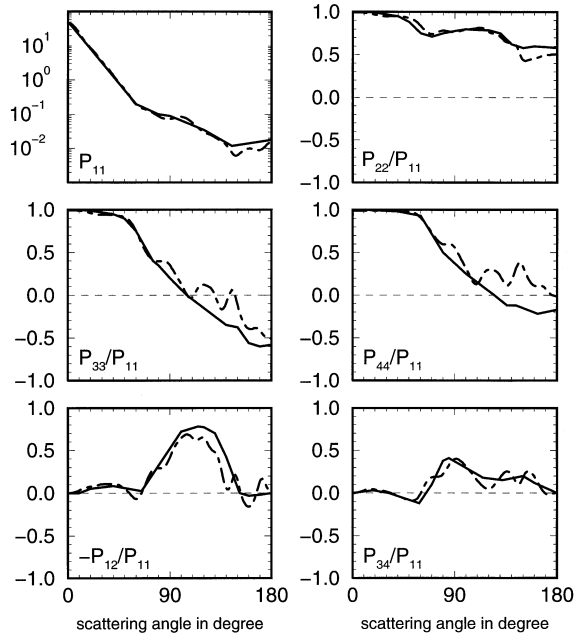

Figure 7. Same as Figure 5, but for an aspect ratio of 5.0.

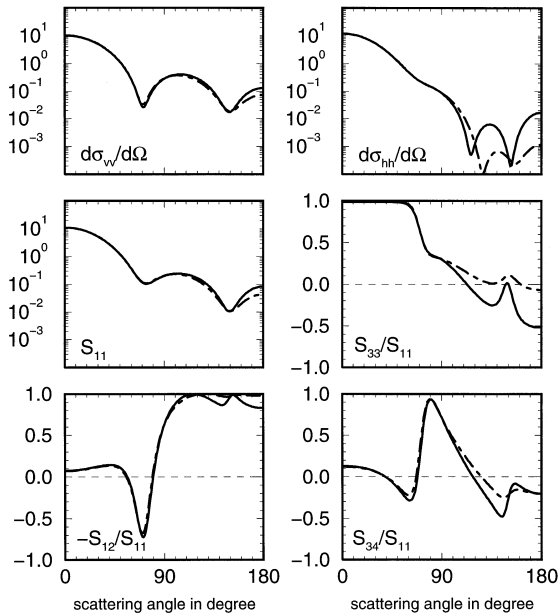

Figure 8. Differential scattering cross-sections and the elements of the Stokes matrix for a circular and a hexagonal cylinder. For the circular cylinder the following parameters have been used: size parameter: 2.75, refractive index: 1.31, aspect ratio: 3.0 (- · -: circular cylinder, –: volume-equivalent hexagonal cylinder of equal length).

volume-equivalent hexagonal cylinder of equal length have been treated by use of our approximation. The results for the fixed orientation perpendicular to the reference plane are given in Figure 8. Significant differences occur only in the back scattering region, especially for $d\sigma_{hh}/d\Omega$. But, if orientation averaging is considered, as depicted in Figure 9, we can hardly distinguish between both geometries. This is due to the relatively small size parameter. The scattering behaviour becomes more dependent on the particle geometry with increasing size parameter. This can be seen by comparing Figures 10 and 11. In Figure 10, the phase matrix is presented for a hexagonal cylinder of size parameter 60. One major difference to the circular cylinder is the occurrence of the 22°-halo in the phase function P_{11} which can be clearly seen by choosing a linear scale. The volume-equivalent circular cylinder of equal length (aspect ratio 3.0) does not show this feature (Figure 11).

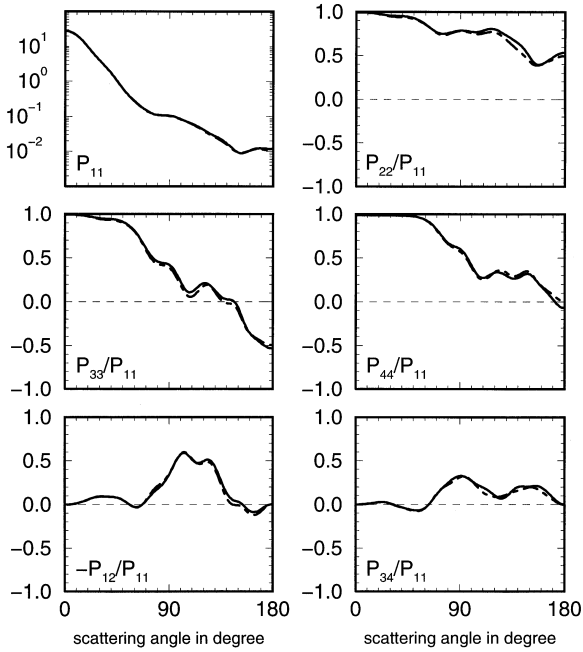

Figure 9. Same as in Figure 7, but elements of the phase matrix (- · -: circular, –: hexagonal).

It is a well established fact that the radiative properties of cirrus clouds are significantly different from that of water clouds. Recent direct measurements of the scattering phase function with a polar nephelometer show an enhanced side scattering at scattering angles of about 100° for ice clouds [34]. The differences are attributed to distinctions in the microphysical properties. While water droplets are approximately spherical, ice crystals occur in a large variety of non-spherical shapes the basic structure of which is hexagonal. In order to investigate the influence of non-sphericity on the phase function, computations for a typical size distribution of hexagonal ice columns and of surface-equivalent spheres were performed (Figure 12). For this comparison the AVHRR-wavelength of $\lambda = 3.775\,\mu m$ was chosen. The crystal dimensions and the corresponding particle densities used in our computations can be found in Table 1. The mentioned phenomenon of an enhanced side scattering in the case of non-spherical particles can be observed within our approximation.

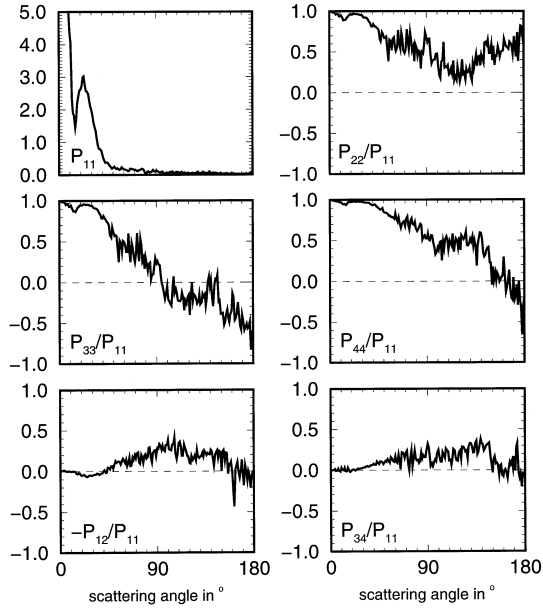

Figure 10. Elements of the phase matrix for randomly oriented finite hexagonal cylinders, with an aspect ratio of 2.7282, size parameter of 60 and refractive index of 1.31.

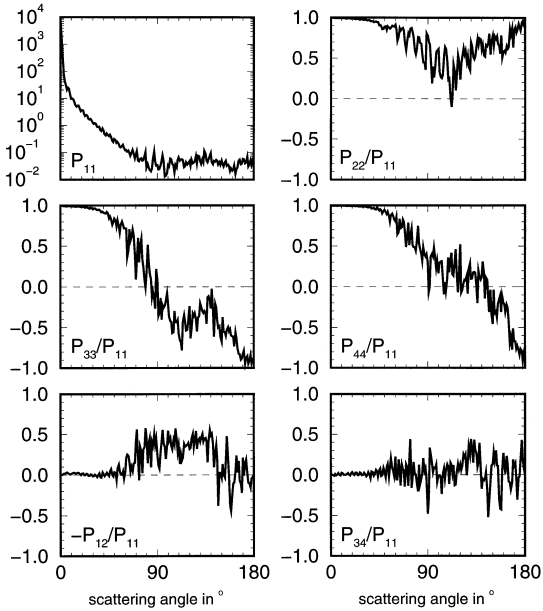

Figure 11. Same as Figure 9, but for the volume-equivalent circular cylinder of equal length (i.e., with an aspect ratio of 3.0).

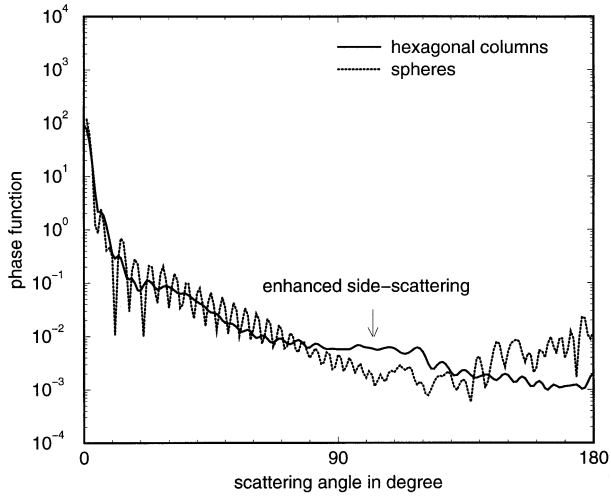

Figure 12. Comparison of the phase functions for a typical size distribution of hexagonal ice columns and of surface-equivalent spheres at a wavelength of 3.775 μm (AVHRR channel No. 3).

Type No.	Column Half-Width in μm	Column Length in μm	Radius of Surface-Equivalent Sphere in μm	Particle Density in m^{-3}
1	1.4	3.5	1.8	$1.69 \cdot 10^5$
2	4.0	10.0	5.1	$3.78 \cdot 10^5$
3	10.0	30.0	13.6	$6.58 \cdot 10^3$
4	22.0	60.0	28.8	$1.47 \cdot 10^3$

Table 1. Typical dimensions of hexagonal ice columns and corresponding particle densities, after [35].

5. CONCLUSIONS

In this contribution, an approximation for scattering on finite non-circular cylinders was presented. It was developed to model the scattering behaviour of hexagonal columns in ice crystal clouds and has already been applied in radiative transfer studies [36]. Characteristic features of hexagonal structures like the 22°-halo as well as the enhanced side scattering of non-spherical particles are retained within the approximation. It can be successfully applied for aspect ratios as low as about 3 without significant errors. Therefore, this approximation can be used as an adequate tool for certain practical applications.

It requires a comparatively small numerical effort since it is based on the solution of the infinite geometry.

REFERENCES

1. Magono, C., and C. W. Lee, "Meteorological classification of natural snow crystals," *Journal of the Faculty of Sciences, Series VII,* Vol. II, 321–335, Hokkaido University, Japan,1966.
2. Auer, A. H., and D. L. Veal, "The dimension of ice crystals in natural clouds," *Journal of the Atmospheric Sciences,* Vol. 27, 919–926, 1970.
3. Gayet, J.-F., F. Auriol, S. Oshchepkov, F. Schröder, C. Duroure, G. Febvre, J.-F. Fournol, O. Crepel, P. Personne, and D. Daugereon, "In situ measurements of the scattering phase functions of stratocumulus, contrails and cirrus," *Geophysical Research Letters,* Vol. 25, 971–974, 1998.
4. Baran, A. J., P. D. Watts, and J. S. Foot, "Potential retrieval of dominating crystal habit and size using radiance data from a dual-view and multiwavelength instrument: A tropical cirrus anvil case," *Journal of Geophysical Research D,* Vol. 103, 6075–6082, 1998.
5. Baran, A. J., J. S. Foot, and D. L. Mitchell, "Ice-crystal absorption: A comparison between theory and implications for remote sensing," *Applied Optics,* Vol. 37, 2207–2215, 1998.
6. Sassen, K., and V. I. Khvorostyanov, "Radar probing of cirrus and contrials: Insights from 2D model simulations," *Geophysical Research Letters,* Vol. 25, 975–978, 1998.
7. Liou, K. N., P. Yang, Y. Takano, K. Sassen, T. Charlock, and W. Arnott, "On the radiative properties of contrail cirrus," *Geophysical Research Letters,* Vol. 25, 1161–1164, 1998.
8. Goodman, J., R. F. Pueschel, E. J. Jensen, S. Verma, G. V. Ferry, S. D. Howard, S. A. Kinne, and D. Baumgartner, "Shape and size of contrails ice particles," *Geophysical Research Letters,* Vol. 25, 1327–1330, 1998.
9. Lawson, R. P., A. J. Heymsfield, S. M. Aulenbach, and T. L. Jensen, "Shapes, sizes and light scattering properties of ice crystals in cirrus and a persistent contrail during SUCCESS," *Geophysical Research Letters,* Vol. 25, 1331–1334, 1998.
10. Macke, A., "Scattering of light by polyhedral ice crystals," *Applied Optics,* Vol. 32, 2780-2788, 1993.
11. Takano, V., and K.-N. Liou, "Radiative transfer in cirrus clouds. Part III: Light scattering by irregular ice crystals," *Journal of the Atmospheric Sciences,* Vol. 52, 818–837, 1995.

12. Muinonen, K., T. Nousiainen, P. Fast, K. Lumme, and J. I. Peltoniemi, "Light scattering by Gaussian random particles: Ray optics approximation," *Journal of Quantitative Spectroscopy and Radiative Transfer,* Vol. 55, 577–602, 1996.
13. Stammes, P., "Light scattering properties of aerosols and the radiation inside a planetary atmosphere," Ph.D. thesis, Free University Amsterdam, The Netherlands, 1989.
14. Kuik, F., "Single scattering of light by ensembles of particles with various shapes," Ph.D. thesis, Free University Amsterdam, The Netherlands, 1992.
15. Takano, Y., K. N. Liou, and P. Minnis, "The effects of small ice crystals on cirrus infrared radiative properties," *Journal of the Atmospheric Sciences,* Vol. 49, 1487–1493, 1992.
16. Travis, L. D., M. I. Mishchenko, and A. Macke, "Scattering of light by polydisperse, randomly oriented, finite circular cylinders," *Applied Optics,* Vol. 35, 4927–4940, 1996.
17. Yang, P., and K.-N. Liou, "Light scattering by hexagonal ice crystals: comparison of finite-difference time domain and geometric optics models," *Journal of the Optical Society of America,* Vol. A12, 162–176, 1995.
18. Yang, P., and K.-N. Liou, "Finite-difference time domain method for light scattering by small ice crystals in three-dimensional space," *Journal of the Optical Society of America,* Vol. A13, 2072–2085, 1996.
19. Aydin, K., and C. Tang, "Millimeter wave radar scattering from model ice crystal distributions," *IEEE Transactions on Geoscience and Remote Sensing,* Vol. 35, 140–146, 1997.
20. Rother, T., and K. Schmidt, "The discretized Mie-formalism for electromagnetic scattering," In J. A. Kong, editor, *Progress in Electromagnetics Research, PIER 17,* 91–183, EMV Publishing, Cambridge, Massachusetts, USA, 1997.
21. Pregla, R., and W. Pascher, "The method of lines," In T. Itoh, editor, *Numerical Techniques for Microwave and Millimeter Wave Passive Structures,* 381–446, John Wiley and Sons, New York, 1989.
22. Rother, T., "Generalization of the separation of variables method for non-spherical scattering on dielectric objects," *Journal of Quantitative Spectroscopy and Radiative Transfer,* Vol. 60, 335-353, 1998.
23. Schmidt, K., T. Rother, and J. Wauer, "The equivalence of applying the extended boundary condition and the continuity conditions for solving electromagnetic scattering problems," *Optics Communications,* Vol. 150, 1–4, 1998.

24. Van de Hulst, H. C., *Light Scattering by Small Particles,* John Wiley and Sons, New York, 1957.
25. Wang, R. T., and H. C. van de Hulst, "Application of the exact solution for scattering by an infinite cylinder to the estimation of scattering by a finite cylinder," *Applied Optics,* Vol. 34, 2811-2821, 1995.
26. Greenberg, J. M., "Some examples of exact and approximative solutions in small particle scattering: A progress report," In T. Gehrels, editor, *Planets, Stars and Nebulae Studied with Photopolarimetry,* 107–134, The University of Arizona Press, Tuscon, Arizona, 1974.
27. Lin, Y.-C., and K. Sarabandi, "Electromagnetic scattering model for a tree trunk above a tilted ground plane," *IEEE Transactions on Geoscience and Remote Sensing,* Vol. 33, 1063–1070, 1995.
28. Wu, T. K., and L. L. Tsai, "Scattering by arbitrarily cross-sectioned layered lossy dielectric cylinders," *IEEE Transactions on Antennas and Propagation,* Vol. 25, 518–524, 1977.
29. Rother, T., and K. Schmidt, "The discretized Mie-formalism for plane wave scattering by dielectric cylinders," *Journal of Electromagnetic Waves and Applications,* Vol. 10, 697–717, 1996.
30. Barton, J. P., "Electromagnetic-field calculations for irregularly shaped, layered cylindrical particles with focused illumination," *Applied Optics,* Vol. 36, 1312–1319, 1997.
31. Kong, J. A., *Electromagnetic Wave Theory,* John Wiley and Sons, New York, 1986.
32. Bohren, C. F., and D. R. Huffman, *Absorption and Scattering of Light by Small Particles,* John Wiley and Sons, New York, 1983.
33. Kuik, F., J. F. de Haan, and J. W. Hovenier, "Single scattering of light by circular cylinders," *Applied Optics,* Vol. 33, 4906–4918, 1994.
34. Larson, H., J.-F. Gayet, G. Febvre, H. Chepfer, and G. Brogniez, "Measurement errors in cirrus cloud microphysical properties," *Annales Geophysicae,* Vol. 16, 266–276, 1998.
35. Strauss, B., "On the climate impact of natural and anthropogenic ice clouds on the regional climate-with special regard to the microphysical influence," Ph.D. thesis, Universität München, 1994.
36. Wendling, P., R. Meerkötter, T. Rother, and S. Havemann, "Remote sensing of cirrus cloud mean effective particle size from AVHRR radiances," In Proceedings of the European Symposium on Aerospace Remote Sensing (ARS), SPIE 3220, Conference on Satellite Remote Sensing of Clouds and the Atmosphere, London, Great Britain, 1997.